

Enhancement of turbulent mixing by a porous obstruction

Dana Duong  and Stavros Tavoularis *

Department of Mechanical Engineering, University of Ottawa, Ottawa, Ontario, Canada K1N 6N5



(Received 10 August 2022; accepted 28 November 2022; published 16 December 2022)

Turbulent diffusion and mixing of heat, introduced passively by a thin ribbon in grid-generated turbulence, were enhanced drastically by a small array of thin cylinders, positioned closely downstream of the ribbon. A multistructure flow region was formed behind the array and relaxed towards grid turbulence, albeit maintaining a turbulence intensity and an integral length scale that were twice as large as those in the absence of the array.

DOI: [10.1103/PhysRevFluids.7.124502](https://doi.org/10.1103/PhysRevFluids.7.124502)

I. INTRODUCTION

Turbulent mixing and diffusion of scalar properties, such as heat and the concentration of an admixture, have been studied extensively, due to their importance in combustion, chemical reactions, spreading of pollutants, and transmission of airborne pathogens [1,2]. Much of our understanding of these phenomena has been based on studies under idealized conditions [3–26], but such findings are also relevant to many practical conditions. Early studies of scalar dispersion from concentrated sources in homogeneous turbulence [27,28] have been adapted to estimate the far-field half-width of a scalar plume, generated by a line source in a uniform stream, as

$$\sigma \approx (2u'_2 L_2 x_1 / \overline{U}_1)^{1/2} \quad \text{for } \sigma \gg L_2, \quad (1)$$

where x_1 is the distance from the source, \overline{U}_1 is the mean velocity, u'_2 is the standard deviation of the transverse turbulent velocity, and L_2 is the transverse integral length scale. More recently, scalar diffusion theory was extended to account for turbulence decay, as would be the case for grid-generated turbulence [29]. In this case, the far-field plume half-width was estimated as

$$\sigma \propto C_\varepsilon^{-1/2} L_1, \quad (2)$$

where L_1 is the streamwise integral length scale and the dissipation parameter is defined in terms of L_1 , the turbulent kinetic energy per unit mass k , and its dissipation rate ε as

$$C_\varepsilon = \varepsilon L_1 / (2k/3)^{3/2}. \quad (3)$$

In isotropic turbulence, $L_2 = L_1$, but, in shear flows, one may generally expect that $L_1 > L_2$. Nevertheless, the scale L_1 was used in Eq. (2) instead of L_2 , because the former is easier to measure, as well as being less sensitive to local inhomogeneity.

In grid turbulence, there is a developing flow region near the grid, where C_ε grows monotonically, followed by a partially developed region and finally a fully developed region, where C_ε is approximately constant [21,29]. Equation (2) implies that, if the far-field condition ($\sigma \gg L_1$) is satisfied at the start of the $C_\varepsilon \approx \text{const}$ region, it will continue being satisfied further downstream, so that the plume will grow at the same rate as the turbulence scale does. The analysis also indicates

*stavros.tavoularis@uottawa.ca

that, if the far-field condition is not satisfied at the start of the $C_\varepsilon \approx \text{const}$ region, it will never be satisfied and the plume will keep growing at a slower rate than L_1 does. Based on these observations, one may develop the following strategy for enhancing the spreading of the plume, thus improving scalar mixing in decaying grid turbulence: Introduce a disturbance close to the source, so that the plume will be wide enough to satisfy the far-field condition early in its evolution and then keep growing at its highest possible rate, which is the rate of growth of L_1 . The choices of geometry and location of the grid, the scalar source, and the obstructions are crucial in implementing this strategy as efficiently as possible. In the following, we will outline the rationale for making the present choices.

First, we chose a grid. We need a grid that has a developing region that is sufficiently long to contain the obstructions, as well as a fully developed region that is sufficiently long for the plume growth to be observable within the wind-tunnel test section. When the grid mesh size M is relatively small, the developing region is essentially nonexistent [21], whereas, when M is relatively large, the highest dimensionless distance x_1/M attainable within the wind-tunnel test section would be small (thus restricting the length of the fully developed region), with the problem compounded by excessive boundary layer interference with the grid turbulence. Among the many grids that were available from previous studies in our laboratory, the one that generated a sizable developing region, a sizable fully developed region, and a core flow that was relatively free of wall effects was found to be a square-mesh perforated plate with a mesh size $M = 50.8$ mm.

In accordance with the previously explained strategy, we placed the scalar source as closely as possible downstream of the perforated plate. In fact, we mounted both the perforated plate and the source on the same frame that was inserted in the wind tunnel. An ideal line source of a scalar would introduce no disturbance to the flow, but such a source would also generate a very narrow plume, which is against the present strategy. Instead of a thin wire, which would approximate a line source, we used a thin ribbon as a source of heat and imposed a twist on it, such that it would introduce a sizable early plume. Of course, we anticipated that the wake generated by the ribbon may also introduce a relatively strong disturbance to the grid turbulence and, consequently, deviation from the conditions that are necessary for the previous plume spread theory to be accurate. Nevertheless, this choice of source appears to be justified, when we consider that our objective is to generate a plume that is as wide as possible near its origin and that grid turbulence would anyway be distorted by the obstruction to be placed downstream of the source.

Following our strategy to widen the plume as far upstream as possible, we placed the obstruction closely downstream of the source. The final, but very crucial, choice was the geometry of the obstruction. If we had introduced a relatively large solid obstruction in the scalar plume, we would have diverted the plume away from the source plane but would have also created a large, scalar-free, wake region. Moreover, the turbulence structure in the wake would be very different from grid turbulence, and the analysis would not hold, even approximately. After considering different possibilities, we decided to use an array of small cylinders, which would act as a porous obstruction, thus allowing the scalar to penetrate the array as well as reducing the disturbance to the grid turbulence. Of course, the turbulence structure behind the array would have contributions from the upstream grid turbulence, as well as contributions of the wakes of the cylinders and the high-speed flows between them. Consequently, this region will have a structure that is the result of more than one distinct turbulence generation mechanism and may be described as multistructure turbulence [30]. To minimize the overall flow disturbance and the pressure drop through the obstruction array, we designed the array such that, instead of being rectangular, it was contained in a triangular envelope, with its apex occupied by a single cylinder facing the source and followed by rows of staggered cylinders, increasing in number. Also to keep the obstruction disturbance relatively small, we set the height of the array to be smaller than the mesh size.

The general goal of this research is to devise a practical method for enhancing scalar mixing in a turbulent flow. In particular, we wished to widen the plume generated by a scalar line source in grid turbulence by inserting a porous obstruction closely behind it. We also wished to explore the

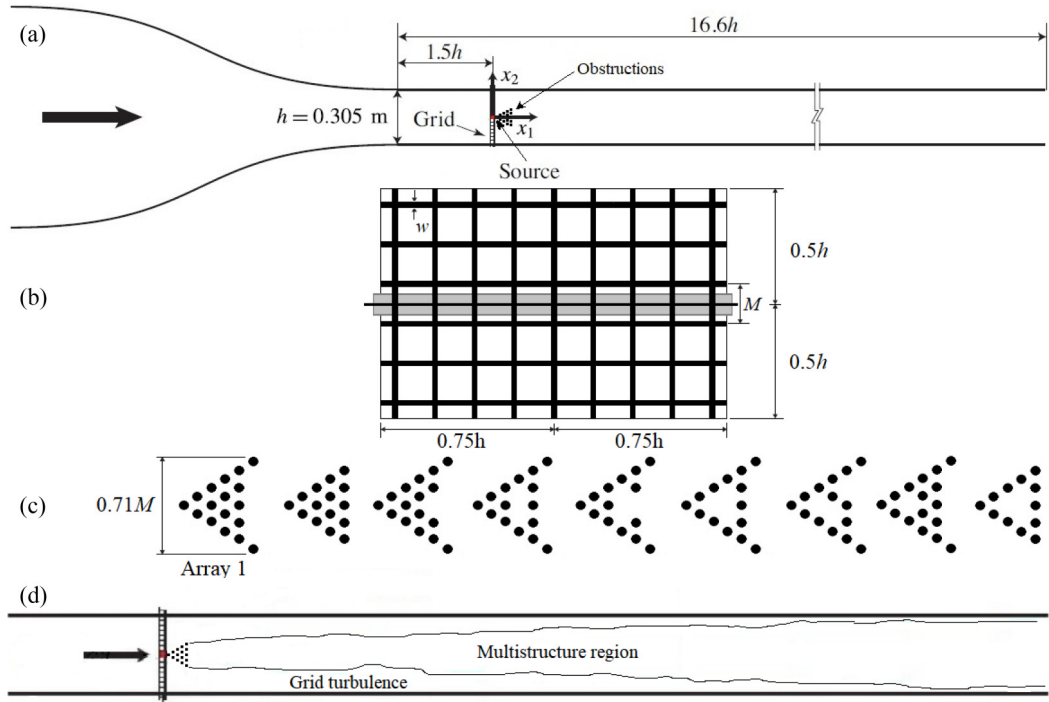


FIG. 1. Sketches of (a) a side view of the general experimental arrangement, (b) a view from upstream of the perforated plate bars (thick black lines), the obstruction projected frontal area (gray rectangle), and the heating ribbon (thin black horizontal line), (c) side views of the different cylinder arrays, and (d) a side view of the different flow regions. The different parts of this figure have different scales.

relationship between the plume spread and the turbulence properties in the multistrukture region behind the obstruction.

II. APPARATUS AND MEASUREMENT PROCEDURES

The experiments were performed in an open-circuit wind tunnel, shown schematically in Fig. 1(a). The test section has a height $h = 305$ mm, a width of $1.5h$, and a length of $16.6h$. Beyond a certain initial length, the test section sidewalls were adjusted to be slightly diverging, to compensate the mean pressure field for boundary layer growth. A square-mesh perforated plate [“grid,” shown in Fig. 1(b)], machined from a 16-gauge steel sheet with a thickness of 1.59 mm and having a mesh size $M = 50.8$ mm ($=0.167h$) and a solid bar width $w = 6.8$ mm (thus a solidity of 0.25), was inserted across the flow. An electrically heated ribbon, made of Nichrome alloy and having a thickness of 0.13 mm and a width of 1.59 mm, was inserted at a location that was 25.4 mm ($=0.50M$) downstream of the grid, to serve as the source of a passive scalar (i.e., temperature rise). The ribbon was twisted by approximately 30° , end to end, with respect to the horizontal plane. The heating power was the same for all reported tests. Arrays of ceramic rods, 3.2 mm in diameter and spaced by 5.5 mm, axis to axis, in equilateral arrangements, were positioned 38 mm ($=0.75M$) downstream of the source, namely, about $1.25M$ downstream of the grid. Each rod spanned the entire width of the test section, and the maximum projected height of the arrays was 36.2 mm, which is equal to $0.71M$. Measurements with the ribbon heated were taken following a warm-up time of 15 min to ensure that the rods had reached constant temperatures. Tests were performed for the nine array configurations that are shown in Fig. 1(c).

Measurements of the streamwise and transverse (i.e., vertical) velocity components and the fluctuating temperature were made with a homemade, three-wire probe. The velocity sensors, arranged in a cross-wire configuration, were made of tungsten and had a diameter of 2.5 μm , a sensing length of 0.85 mm, and a separation distance of 0.5 mm. The length-to-diameter ratio was 340, which is sufficiently large for end conduction effects to be negligible [31]. The temperature sensor (“cold wire”) was made of platinum and had a diameter of 0.6 μm and a length-to-diameter ratio of 800; this sensor was etched from Wollaston wire and spot welded onto the prongs. The cold wire was supplied with a current of 0.3 mA by a low-noise, high-gain homemade circuit. The mean temperature close to the three-wire probe was measured with a miniature thermistor. The hot-wire signals were corrected for temperature effects, using an instantaneous temperature value that was the sum of the time-averaged temperature, measured with the thermistor, and the mean-free temperature fluctuation, measured with the cold wire. The reported temperature rise in the heated flow was the difference between the locally measured temperature and the temperature upstream of the heated source, measured with a precalibrated resistance temperature detector (RTD). The hot-wire and cold-wire signals were low-pass filtered with analog filters, having cutoff frequencies of 14 and 4 kHz, respectively, digitized at a rate of 30 kHz and recorded over 30 s for each test. The cross-wire probe was calibrated *in situ* using a velocity-pitch-map calibration method [32].

The streamwise integral time scale T_1 was determined by integrating the temporal autocorrelation coefficient of the streamwise velocity fluctuations to its first zero crossing. The streamwise integral length scale was then estimated as $L_1 = T_1 \bar{U}_1$. The derivative $(\partial u_1 / \partial r)^2$ was calculated by extrapolating corresponding finite differences to a zero time lag. The Taylor microscale was calculated with the use of Taylor’s frozen flow approximation as $\lambda = \bar{U}_1 [u_1'^2 / (\partial u_1 / \partial r)^2]^{1/2}$, and the turbulence Reynolds number was calculated as $\text{Re}_\lambda = u_1' \lambda / \nu$, where ν is the kinematic viscosity of air. Lastly, the Taylorian diffusivity was calculated as $D = u_2'^2 L_1 / 2$.

III. RESULTS AND DISCUSSION

All measurements were taken at a fixed inlet velocity of $U_\infty = 10.0$ m/s, calculated from the mean pressure difference across the wind-tunnel contraction. In the absence of a grid, heating source, and flow obstructions, velocity fluctuations in the streamwise and transverse directions were found to be about 0.1%. The Reynolds number, based on the grid mesh size, was $\text{Re}_M = U_\infty M / \nu \approx 34\,000$.

Preliminary measurements downstream of each of the nine cylinder arrays showed that, consistently with previous work [21,33], the mean temperature profiles had a nearly Gaussian shape. The peak of the obstructed temperature profile was substantially lower than that in unobstructed grid turbulence, while the plume was substantially wider. The additional spread of heat in the presence of the obstruction is attributed to two interacting, but distinct, effects. First, the warm wake of the source is either split by the first cylinder or diverted towards one side of it, in both cases tending to displace heated fluid away from the source plane. This process is repeated, as the displaced warm fluid reaches the second and subsequent cylinders. One is also reminded that the near field of a square-mesh grid consists of square jets, surrounded by short horizontal and vertical wakes, so that the flow reaching the obstruction is strongly three dimensional. Second, the cylinders produce additional turbulent fluctuations, which are superimposed on the grid turbulence, as well increasing the size of the energy-containing motions; both effects enhance turbulent diffusion. The effect of the obstructions on the plume spread is quite strong, despite the fact that the frontal projection of a full cylinder array is merely $0.076h$ in height.

Most effective in reducing the peak temperature rise was array 1, and so all measurements reported here were taken for this configuration. Profiles of the mean temperature rise $\Delta \bar{T}$ at three streamwise stations are shown in Fig. 2. These values have been normalized by a constant reference temperature rise $\Delta T_{\text{ref}} = 0.44$ K, which is equal to the peak mean temperature rise in the unobstructed flow at $x_1/M = 6$. Although the unobstructed plume extended entirely within the flow core region (namely, it did not reach the boundary layers along the top and bottom walls), the

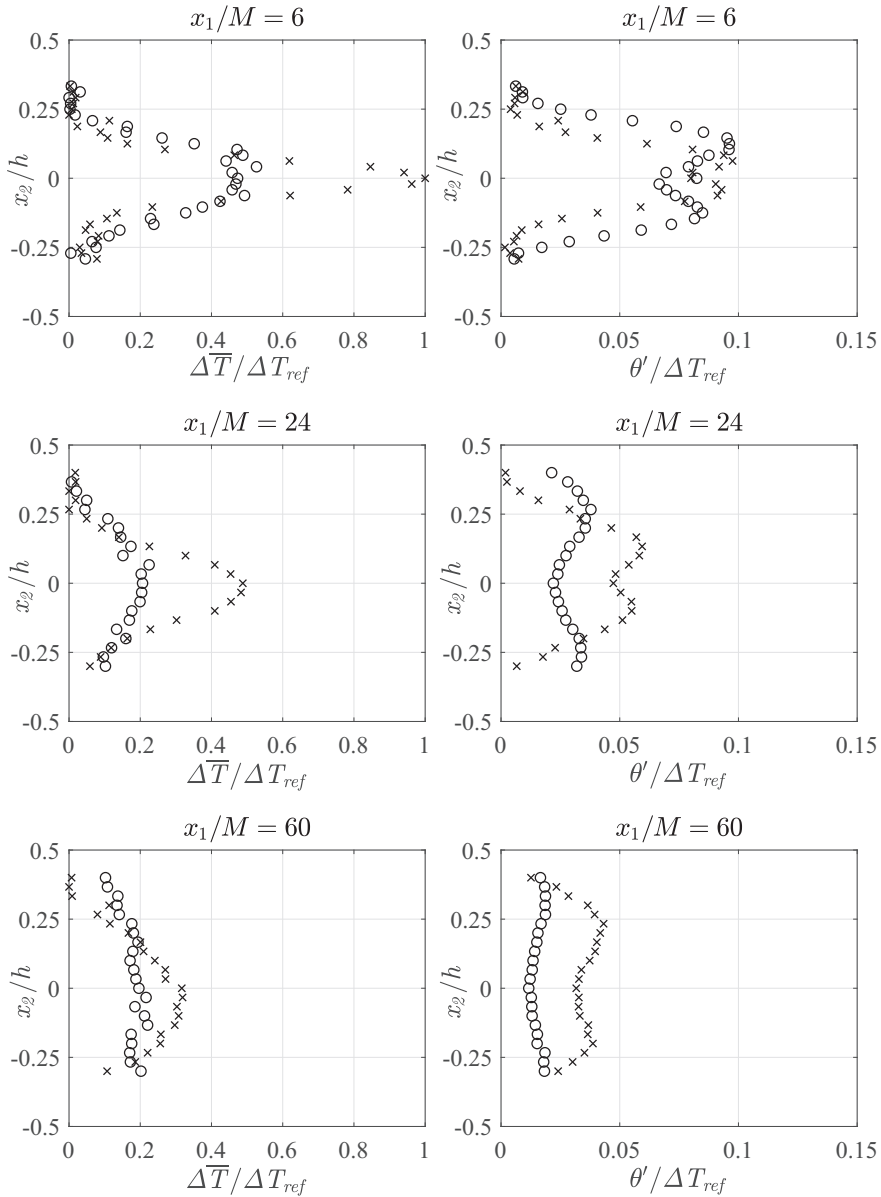
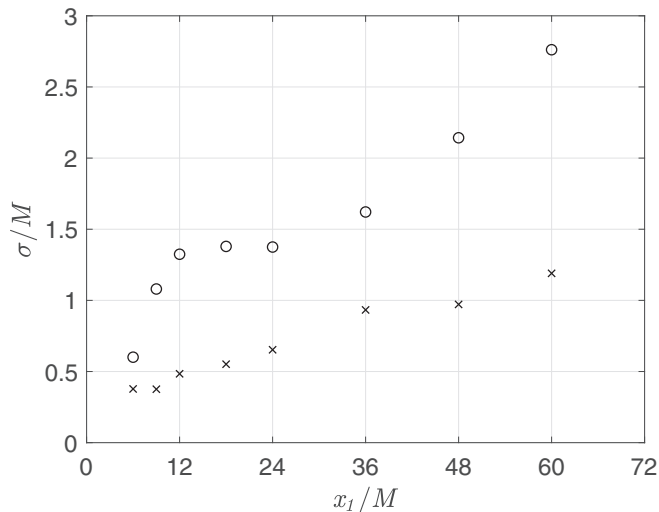


FIG. 2. Normalized mean temperature and temperature fluctuation profiles without (\times) and with (\circ) the obstructions at three streamwise locations; the reference temperature rise was $\Delta T_{ref} = 0.44$ K.

obstructed plume grew wider than the core, encroaching into the boundary layers at the furthest station, where $x_1/M = 60$. Figure 2 also presents the transverse profiles of the normalized standard deviation θ' of the temperature fluctuations, at the same three streamwise locations. Dual peaks can be seen in both the unobstructed and obstructed flows, but, in the obstructed flow, the fluctuations spread further in the transverse direction and had a smaller nonuniformity. As shown in Fig. 3, the obstructed plume was roughly twice as wide as the unobstructed one. Figure 2 indicates that the obstruction intensified scalar mixing to the point that, roughly speaking, the mean temperature rise in the entire test section far away from the source exceeded half of its peak values in the


 FIG. 3. Plume spread without (\times) and with (\circ) the obstructions.

unobstructed case. In contrast, throughout the unobstructed flow, there were significant parts of the test section where there was no temperature rise at all. All things considered, we may confidently assert that the obstruction was quite effective in spreading and mixing the scalar.

To understand the effect of the obstructions, we compared the turbulence properties in their presence with those in their absence. Measured values of turbulence properties along the centerline, without and with the cylinder array, are listed in Table I, and representative vertical profiles of such properties are shown in Fig. 4. It should be noted that the various profiles near the grid are not expected to be two dimensional, but to have significant spanwise nonuniformity, generated by the vertical bars of the grid and the ribbon twist. It is also noted that the heating ribbon had a

TABLE I. Values of various properties at selected locations along the centerline; the values of P are at $x_2/h = 0.125$, where this property was at or near its peak.

x_1/M	Grid only			Grid + array 1		
	6	24	60	6	24	60
$\Delta T/\Delta T_{\text{ref}}$	1	0.488	0.317	0.473	0.206	0.196
$\theta'/\Delta T_{\text{ref}}$	0.160	0.095	0.063	0.164	0.044	0.023
σ/M	0.378	0.653	1.19	0.601	1.375	2.762
\bar{U}_1/U_∞	0.857	0.949	0.967	0.701	0.903	0.941
u'_1/U_∞	0.094	0.035	0.020	0.165	0.068	0.036
u'_2/U_∞	0.080	0.032	0.018	0.198	0.065	0.030
$-\overline{u_1 u_2}/u'_1 u'_2$	0.017	-0.119	-0.114	0.000	0.005	-0.001
L_1/M	0.227	0.363	0.508	0.291	0.732	0.936
D (m ² /s)	0.004	0.001	0.0004	0.029	0.007	0.002
λ/M	0.029	0.178	0.339	0.029	0.179	0.337
Re_λ	89	68	67	158	132	117
P (m ² /s ³)	11.0	0.40		42	1.8	
$-S$	0.36	0.42	0.40	0.53	0.43	0.50
F	5.4	5.0	4.4	7.3	6.5	5.6

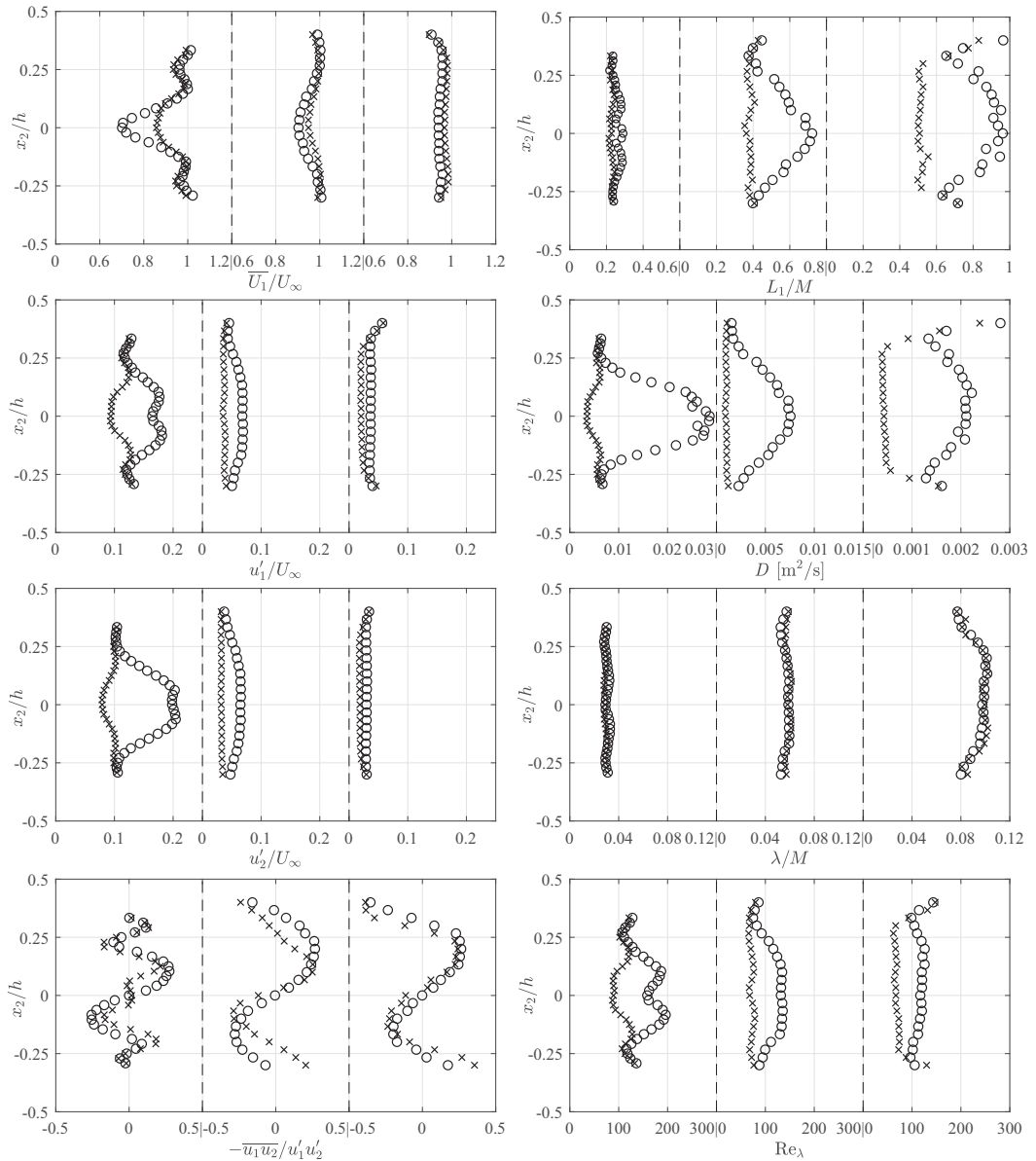


FIG. 4. Transverse profiles of the main turbulence properties without (\times) and with (\circ) the obstructions at three streamwise locations; the axis scales for L_1 and D at each location have been adjusted to make the values readable.

measurable momentum wake, although we found no signs of buoyancy effects due to the heating. The main observations that can be based on these results are summarized as follows.

(a) Closely downstream of it, the obstruction increased the mean velocity deficit along the centerline to a level that was well above the already significant level in the absence of the obstruction, which is attributed to the grid bars and the ribbon wake. This deficit diminished with downstream distance, so that the mean flow in the core became nearly uniform at $x_1/M = 60$. At that location, the boundary layers on the top and bottom walls may be seen to occupy roughly a quarter of the

cross section each, with very weak velocity peaks persisting at the boundary layer edges; these peaks are interpreted to be remnants of upstream flow maxima between bar-generated wakes.

(b) The streamwise turbulent velocity fluctuation level behind the obstruction was nearly twice the unobstructed value in the entire test section, which means that the obstruction generated a permanent increase in turbulence level.

(c) The transverse turbulent velocity fluctuations behind the obstruction followed the same overall patterns as the streamwise fluctuations. It is interesting to note that, at $x_1/M = 6$, u'_2 was somewhat larger than u'_1 , as the obstruction diverted flow away from the centerline. Further downstream, the ratio u'_1/u'_2 , both without and with obstructions, settled at a level in the range 1.1–1.2, which is somewhat larger than typical values in turbulence generated by grids with solidities that are higher than the present one [34]. In the near-wake of the obstruction, the turbulence intensity u'_1/\overline{U}_1 exceeded 20%. This brings into question the validity of Taylor's frozen flow approximation, but we note that a recent study on this issue [35] concluded that Taylor's approximation stands for $u'_1/\overline{U}_1 \lesssim 25\%$.

(d) Unlike isotropic turbulence, the present flow had a measurable Reynolds shear stress, which is attributed to the combined wakes of the ribbon and the obstruction. The shear stress correlation coefficient was only mildly affected by the obstruction. It is interesting to note that, without and with the obstruction, this coefficient was negligible along the streamline and reached peak values of about ± 0.25 at about $x_2/h \approx \pm 0.125$, which points to persisting mild inhomogeneity and anisotropy throughout the measuring section. The peak shear stress correlation coefficient was smaller in magnitude than its value in outer turbulent boundary layers and in uniformly sheared turbulence, where it is about 0.4.

(e) In view of the appreciable mean shear and shear stress in parts of the flow, we examined the turbulence production $P = -\overline{u_1 u_2} d\overline{U}_1/dx_2$. In both the unobstructed and obstructed flows, P was negligible along the centerline, but it reached distinct peaks at about $x_2/h \approx \pm 0.125$. The peak production was up to a third of a corresponding rough estimate of the local turbulent kinetic energy dissipation rate and up to nearly half the dissipation value in the obstructed flow. By comparison, the production-to-dissipation ratio in uniformly sheared turbulence is about two-thirds [18].

(f) The obstruction nearly doubled the integral length scale, and such increase was maintained downstream.

(g) The obstruction increased drastically the turbulent diffusivity $D \approx u_2^2 L_1/2$ in its wake. Close to the obstruction, the increase was by an order of magnitude and peaked on the centerline, but, further downstream, the turbulent diffusivity maintained a fairly uniform value in the flow core, which was roughly four times the corresponding unobstructed value. This increase in D is consistent with the drastic enhancement of scalar mixing.

(h) The Taylor microscale was essentially unaffected by the obstruction; this indicates that the obstruction increased both the velocity fluctuations and their temporal derivative by the same amount. Nevertheless, there was a very small correlation ($\lesssim 0.1$ for $x_1/M \geq 24$) between the velocity and its derivative. A physical justification for the lack of influence of the obstruction on the Taylor microscale remains to be found.

(i) The turbulence Reynolds number was roughly doubled by the obstruction, as a result of the increase of the turbulence level.

(j) As a final note, Fig. 5 shows representative profiles of the skewness S and flatness F factors of the streamwise velocity derivative, which are indicators of the fine structure. Away from the grid ($x_1/M \geq 24$), S takes values in the vicinity of -0.5 in both the unobstructed and the obstructed flows; such values are typical for fully developed turbulence at moderate Reynolds numbers [36–40]. However, closer to the grid ($x_1/M = 6$), S takes values that are measurably lower than the value -0.5 without the obstruction and closer to -0.5 with the obstruction; thus it appears that the effect of the obstruction is to accelerate the development of the turbulence structure. Moreover, the obstruction increases systematically the flatness factor throughout the test section, which is consistent with the increase in Re_λ and indicates an enhancement of the internal intermittency of the turbulence. It should be noted that, at the furthest downstream station ($x_1/M = 60$), the

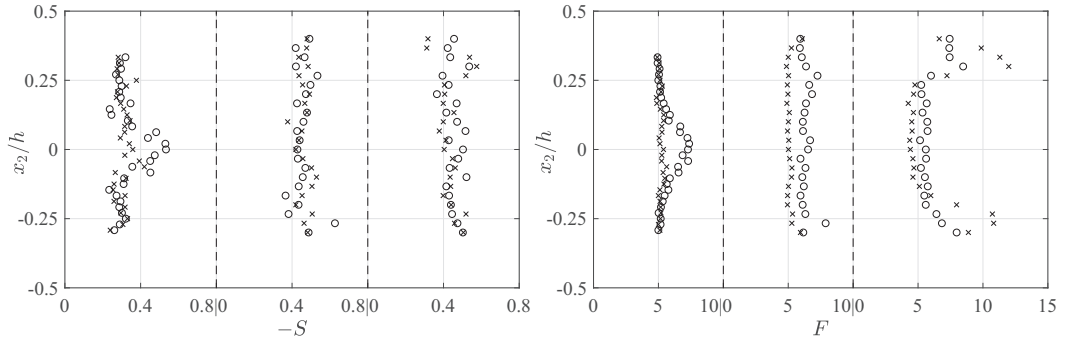


FIG. 5. Transverse profiles of the skewness and flatness factors of the streamwise velocity derivative without (\times) and with (\circ) the obstructions. The axis scale of F at each location has been adjusted to make the values readable.

flatness factor is drastically larger outside the flow core ($|x_2/h| > 0.25$) than within the core $-0.25 \leq x_2/h \leq 0.25$; this is attributed to the intermittency between grid turbulence and turbulence in the boundary layers developing along the test section walls.

IV. CONCLUSIONS

In this paper, we found that a small array of thin cylinders, acting as a localized, porous, flow obstruction, enhanced drastically turbulent diffusion and mixing of a passive scalar injected from a line source in grid turbulence. The unobstructed scalar plume was confined within the test section core region, whereas the obstructed plume penetrated the boundary layers on the test section walls. This is further confirmed by the fact that the plume spread in the obstructed flow was twice as large as that in unobstructed grid turbulence. Transverse profiles of turbulence properties indicated that a multistructure flow region was formed behind the array and relaxed towards grid turbulence, albeit maintaining permanent increases in turbulence level, integral length scale, and turbulent diffusivity.

ACKNOWLEDGMENT

Funding for this research was provided by the Natural Sciences and Engineering Research Council of Canada, Grant No. RGPIN-2017-03835.

-
- [1] P. E. Dimotakis, Turbulent mixing, *Annu. Rev. Fluid Mech.* **37**, 329 (2005).
 - [2] Z. Warhaft, Passive scalars in turbulent flows, *Annu. Rev. Fluid Mech.* **32**, 203 (2000).
 - [3] E. Germaine, L. Mydlarski, and L. Cortelezzi, Evolution of the scalar dissipation rate downstream of a concentrated line source in turbulent channel flow, *J. Fluid Mech.* **749**, 227 (2014).
 - [4] U. Karnik and S. Tavoularis, Measurements of heat diffusion from a continuous line source in a uniformly sheared turbulent flow, *J. Fluid Mech.* **202**, 233 (1989).
 - [5] G. I. Taylor, Statistical theory of turbulence. Parts I–IV, *Proc. R. Soc. London A* **20**, 151 (1935).
 - [6] S. P. Arya, *Air Pollution Meteorology and Dispersion* (Oxford University Press, Oxford, 1999), Vol. 6.
 - [7] D. R. Webster, P. J. W. Roberts, and L. Ra'ad, Simultaneous DPTV/PLIF measurements of a turbulent jet, *Exp. Fluids* **30**, 65 (2001).
 - [8] D. R. Webster, S. Rahman, and L. P. Dasi, Laser-induced fluorescence measurements of a turbulent plume, *J. Eng. Mech.* **129**, 1130 (2003).

- [9] S. Rahman and D. R. Webster, The effect of bed roughness on scalar fluctuations in turbulent boundary layers, *Exp. Fluids* **38**, 372 (2005).
- [10] I. Nakamura, Y. Sakai, and H. Tsunoda, On conditional statistics of the diffusion field of matter by a point source plume in uniform mean shear flow, *JSME Int. J. Ser. II* **32**, 180 (1989).
- [11] A. Borg, J. Bolinder, and L. Fuchs, Simultaneous velocity and concentration measurements in the near field of a turbulent low-pressure jet by digital particle image velocimetry–planar laser-induced fluorescence, *Exp. Fluids* **31**, 140 (2001).
- [12] K. Sakakibara, J. Hishida, and M. Maeda, Vortex structure and heat transfer in the stagnation region of an impinging plane jet (simultaneous measurements of velocity and temperature fields by digital particle image velocimetry and laser-induced fluorescence), *Int. J. Heat Mass Transfer* **40**, 3163 (1997).
- [13] R. A. Lavertu and L. Mydlarski, Scalar mixing from a concentrated source in turbulent channel flow, *J. Fluid Mech.* **528**, 135 (2005).
- [14] H. Stapountzis, B. L. Sawford, J. C. R. Hunt, and R. E. Britter, Structure of the temperature field downwind of a line source in grid turbulence, *J. Fluid Mech.* **165**, 401 (1986).
- [15] C. Vanderwel and S. Tavoularis, Measurements of turbulent diffusion in uniformly sheared flow, *J. Fluid Mech.* **754**, 488 (2014).
- [16] M. S. Anand and S. B. Pope, Diffusion behind a line source in grid turbulence, in *Turbulent Shear Flows 4*, edited by L. Bradbury, F. Durst, B. Launder, F. Schmidt, and J. Whitelaw (Springer, New York, 1985), pp. 46–61.
- [17] J. Lepore and L. Mydlarski, Lateral dispersion from a concentrated line source in turbulent channel flow, *J. Fluid Mech.* **678**, 417 (2011).
- [18] S. Tavoularis and S. Corrsin, Experiments in nearly homogenous turbulent shear flow with a uniform mean temperature gradient. Part 1, *J. Fluid Mech.* **104**, 311 (1981).
- [19] S. Tavoularis and S. Corrsin, Experiments in nearly homogeneous turbulent shear flow with a uniform mean temperature gradient. Part 2. The fine structure, *J. Fluid Mech.* **104**, 349 (1981).
- [20] Z. Warhaft, The interference of thermal fields from line sources in grid turbulence, *J. Fluid Mech.* **144**, 363 (1984).
- [21] J. Nedić and S. Tavoularis, Measurements of passive scalar diffusion downstream of regular and fractal grids, *J. Fluid Mech.* **800**, 358 (2016).
- [22] M. K. Chung and N. H. Kyong, Measurement of turbulent dispersion behind a fine cylindrical heat source in a weakly sheared flow, *J. Fluid Mech.* **205**, 171 (1989).
- [23] M. S. Uberoi and S. Corrsin, Diffusion of heat from a line source in isotropic turbulence, NACA Technical Note No. 2710 (National Advisory Committee for Aeronautics, Washington, DC, 1952).
- [24] J. E. Fackrell and A. G. Robins, Concentration fluctuations and fluxes in plumes from point sources in a turbulent boundary layer, *J. Fluid Mech.* **117**, 1 (1982).
- [25] A. Townsend, The diffusion behind a line source in homogeneous turbulence, *Proc. R. Soc. London A* **224**, 487 (1954).
- [26] L. Mydlarski, L. Danaila, and R. A. Lavertu, Isotropy of the temperature field downstream of a line source in turbulent channel flow, in *Advances in Turbulence XI: Proceedings of the 11th EUROMECH European Turbulence Conference*, Springer Proceedings in Physics Vol. 117 (Springer, New York, 2007), pp. 500–502.
- [27] G. I. Taylor, Diffusion by continuous movements, *Proc. London Math. Soc.* **20**, 196 (1921).
- [28] G. K. Batchelor, Diffusion in a field of homogeneous turbulence. I. Eulerian analysis, *Aust. J. Chem.* **2**, 437 (1949).
- [29] S. Tavoularis and J. Nedić, Taylorian diffusion in mildly inhomogeneous turbulence, *Int. J. Heat Fluid Flow* **67**, 116 (2017).
- [30] J. Nedić and S. Tavoularis, A case study of multi-structure turbulence: Uniformly sheared flow distorted by a grid, *Int. J. Heat Fluid Flow* **72**, 233 (2018).
- [31] J. D. Li, B. J. McKeon, W. Jiang, J. F. Morrison, and A. J. Smits, The response of hot wires in high Reynolds-number turbulent pipe flow, *Meas. Sci. Technol.* **15**, 789 (2004).
- [32] R. M. Lueptow, K. S. Breuer, and J. H. Haritonidis, Computer-aided calibration of X-probes using a look-up table, *Exp. Fluids* **6**, 115 (2004).

- [33] G. I. Taylor, The spectrum of turbulence, *Proc. R. Soc. London A* **164**, 476 (1938).
- [34] G. Comte-Bellot and S. Corrsin, The use of a contraction to improve the isotropy of grid-generated turbulence, *J. Fluid Mech.* **25**, 657 (1966).
- [35] M. Wilczek, H. Xu, and Y. Narita, A note on Taylor's hypothesis under large-scale flow variation, *Nonlinear Processes Geophys.* **21**, 645 (2014).
- [36] Y. Zheng, K. Nagata, and T. Watanabe, Energy dissipation and enstrophy production/destruction at very low Reynolds numbers in the final stage of the transition period of decay in grid turbulence, *Phys. Fluids* **33**, 035147 (2021).
- [37] R. A. Antonia and A. J. Chambers, On the correlation between turbulent velocity and temperature derivatives in the atmospheric surface layer, *Boundary-Layer Meteorol.* **18**, 399 (1980).
- [38] J. C. Bennett and S. Corrsin, Small Reynolds number nearly isotropic turbulence in a straight duct and a contraction, *Phys. Fluids* **21**, 2129 (1978).
- [39] R. M. Kerr, Higher-order derivative correlations and the alignment of small-scale structures in isotropic numerical turbulence, *J. Fluid Mech.* **153**, 31 (1985).
- [40] C. W. Van Atta and R. A. Antonia, Reynolds number dependence of skewness and flatness factors of turbulent velocity derivatives, *Phys. Fluids* **23**, 252 (1980).